Mechanical Properties of Short Sisal Fiber-Reinforced Polypropylene Composites: Comparison of Experimental Data with Theoretical Predictions

P. V. Joseph,[1] G. Mathew,[2] K. Joseph,[1] S. Thomas,[3] P. Pradeep[4]

[1]*Post Graduate Department of Chemistry, St. Berchmans' College Changanacherry, Kottayam, Kerala, India*
[2]*Department of Chemistry, CMS College, Kottayam, Kerala, India*
[3]*School of Chemical Sciences, Mahatma Gandhi University, Kottayam, Kerala, India*
[4]*Condensed Matter Physics Lab, Department of Physics, SN College, Kollam, India*

Received 25 August 2000; accepted 22 April 2002
Published 11 February 2003 in Wiley InterScience (www.interscience.wiley.com). DOI 10.1002/app.11498

ABSTRACT: Sisal fibers were used for the reinforcement of a polypropylene (pp) matrix. Composites consisting of polypropylene reinforced with short sisal fibers were prepared by melt-mixing and solution-mixing methods. A large amount of fiber breakage was observed during melt mixing. The fiber breakage analysis during composite preparation by melt mixing was carried out using optical microscopy. A polynomial equation was used to model the fiber-length distribution during melt mixing. The experimental mechanical properties of sisal/PP composites were compared with existing theoretical models such as the modified rule of mixtures, parallel and series models, the Hirsch model, and the Bowyer–Baders model. The dependence of the tensile strength on the angle of measurement with respect to fiber orientation also was modeled. © 2003 Wiley Periodicals, Inc. J Appl Polym Sci 88: 602–611, 2003

Key words: mechanical properties; fibers; polypropylene; composites

INTRODUCTION

In the field of composites, the fiber reinforcement of matrices was initially developed using man-made fibers such as glass, carbon, and aramid to take advantage of their high tensile moduli.[1] Over the last few years, many works have been dedicated to fibers of vegetable origin, with the scope of replacing man-made fibers.[2] Numerous reasons support this choice: As a material source, vegetable fibers are available worldwide, renewable, and biodegradable. They may also represent an economical interest for the agricultural sector. Concerning their intrinsic properties, these fibers have a specific weight half that of glass fibers and a tensile modulus for the ultimate fibril almost as high as for aramid fibers.[3] Moreover, they cause no damage by abrasion to the processing machines as glass fibers do, which also give a high amount of ashes on combustion.[1] The biodegradability of natural fibers can contribute to a healthy ecosystem, while their low costs and high performance are able to fulfill the economic interest of industries.[4]

In recent years, short natural fiber-reinforced polymer composites have gained wide importance due to the advantages they impart in processing and low cost coupled with high strength.[5] For better processability, these composite materials are often filled with short discontinuous fibers oriented in the direction of the applied load in order to take full advantage of the reinforcing property of the fiber.[6–8] Since natural fibers are strong, light in weight, abundant, nonabrasive, nonhazardous, and inexpensive, they can serve as an excellent reinforcing agent for plastics.[9,10] At present, natural vegetable fibers (NVFs) are used in composites, where high strength and stiffness are not of first priority. NVFs reduce the mass of the composite, because they have a low density. Their production is economical, with low requirements on equipment, and they can easily by recycled.[11] Natural fiber composites combine good mechanical properties with a low specific mass.[12]

Over the past decade, cellulosic fillers of a fibrous nature have been of great interest as they would give composites with improved mechanical properties compared to those containing nonfibrous fillers.[13–15] Extensive research studies have been carried out over the last few years in the field of natural fiber-reinforced thermoplastics. These include the interesting works of Kokta and coworkers.[16–22] Felix and Gatenholm[23] reported the effect of a compatibilizing agent and the nature of adhesion in composites of cellulose fibers and polypropylene (PP). Among the various natural fibers, sisal fiber possesses a moderately high specific strength and stiffness and can be used as a

Correspondence to: S. Thomas (sabut@md4.vsnl.net.in).

TABLE I
Physical and Mechanical Properties of PP and Sisal Fiber

Properties	PP	Sisal fiber
Melt flow index (g/10 min)	3	—
Density (g/cm^3)	0.9	1.45
Cellulose content (%)	—	85–88
Lignin content (%)	—	4–5
Tensile strength (MPa)	35	400–700
Tensile modulus (MPa)	498	9000–20,000
Elongation at break (%)	10.33	5–14

reinforcing material in polymeric resin matrices to make useful structural composite materials.[13] Sisal fiber is a lignocellulosic material extracted from the plant *Agave sisalana* and is available in quantity in the southern parts of India. The incorporation of sisal fiber into plastics and elastomers to obtain cost reduction and reinforcement has been reported by various workers. Parameswaran and Abdulkalam[24] investigated the feasibility of developing polymer-based composites using sisal fiber. Pavithran et al.[25] reported the impact properties of unidirectionally oriented sisal fiber composites. Thomas and coworkers reported on the use of sisal and pineapple fibers as a potential reinforcing agent in polyethylene, thermosets (epoxy resin, phenol–formaldehyde, polyester), polystyrene, and natural rubber.[25–30] Joseph and coworkers,[31,32] therefore, carried out a detailed investigation on sisal fiber-reinforced PP composites with special reference to the effects of fiber length, processing conditions, fiber loading, and interface adhesion. In this article, we made an effort to describe the relative ability of some selected already-existing mathematical models—the modified rule of mixtures, parallel, series, Hirsch, and Bowyer–Baders—to predict the variation in the mechanical properties of PP composites with increasing loading of short sisal fiber. The fiber-length distribution and directional property of short sisal fiber-reinforced PP composites were also modeled.

EXPERIMENTAL

Materials

Isotactic PP (Koylene M3060) was supplied by IPCL (Baroda, India). Sisal fiber (*Agave sisalana*) was obtained from local sources. The physical and mechanical properties of PP and sisal fiber are given in Table I. The fiber was washed thoroughly with water and dried in an air oven at 80°C for 6 h, before being chopped into the desired lengths ranging from 1 to 30 mm for preparation of the composites.

Fiber treatment[32]

The PMPPIC used for this work was supplied by Aldrich Chemical Co. (Milwaukee, WI). To the sisal fibers dipped in chloroform (distilled) in a 500-mL RB flask, varying percentages of PMPPIC (5–12% by weight of the fiber) in chloroform (50 mL) was added to a pressure equalizing funnel. The addition continued for 30 min and the contents were stirred using a magnetic stirrer. The whole assembly was immersed in a water bath at 70°C before the addition of PMPPIC. After the complete addition of PMPPIC, the reaction was allowed to continue for 2 h more. The urethane-modified fibers were collected.

Composite preparation

The PP–sisal composites were prepared by either melt mixing or solution mixing. In the melt-mixing method, the fiber was added to a melt of PP and mixing was performed in a Haake Rheocord mixer. To optimize the mixing parameters, composites were prepared by varying the mixing time, rotor speed, and chamber temperature. The mix was taken out from the mixer while hot and then subjected to sheeting using a two-roll mill.

Rectangular specimens measuring 150 × 150 × 2.5 mm were prepared by compression molding at a pressure of about 8 MPa and at a temperature of 170°C. They were then cut into specimens of size 120 × 12 × 2.5 mm.

In the solution-mixing method, a technique developed by our group,[31,33] the fiber was mixed with a viscous slurry of PP in a toluene/xylene mixture (1:1 ratio) that was prepared by adding the toluene/xylene mixture to a melt of the polymer. The mix was then completely dried in an air oven to remove the solvent and then was subjected to extrusion through a hand-operated injection-molding machine. Composite sheets of dimensions 120 × 12 × 2.5 mm were prepared by a compression-molding technique.

Preparation of oriented fiber composites

The specimens of oriented fiber composites were prepared by a combination of injection-molding and compression-molding techniques as reported elsewhere.[26] The composite was first processed to obtain 4-mm-thick cylindrical rods using an injection-molding machine. Rectangular specimens measuring 120 × 26.5 × 2.5 mm were prepared by aligning the extrudate (120-mm long and 4-mm diameter) in a leaky mold and then compression molding at a pressure of about 8 MPa and at a temperature of 170 ± 5°C. The specimens were removed after cooling the mold below 50°C.

Mechanical testing

Rectangular specimens were prepared as reported elsewhere[26] for carrying out tensile testing using an

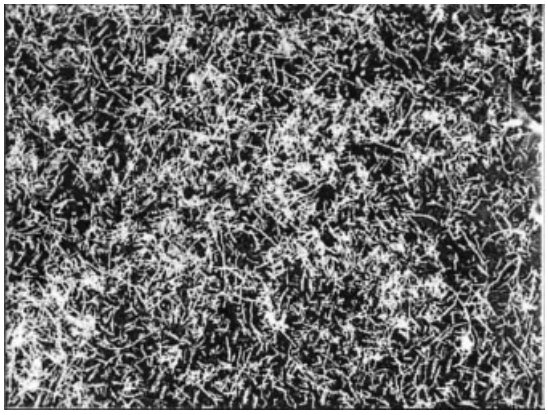

Figure 1 Optical photograph of fibers extracted from melt-mixed composite showing extent of fiber breakage.

electronic tensile testing machine TNE series 9200 at a crosshead speed of 50 mm min^{-1} and a gauge length of 50 mm. The tensile modulus of the composites was calculated from the load-displacement curve.

Fiber breakage analysis

During melt mixing in a Rheocord mixer, fibers undergo a considerable amount of breakage.[31] The extent of fiber breakage in a melt-mixed composite is evident from the optical photograph shown in Figure 1. Here, fibers were extracted from the melt-mixed composite by dissolving the PP matrix in a toluene/xylene mixture at the ratio 2:1 as a solvent and measuring the fiber lengths using a traveling microscope.

THEORETICAL ASPECTS

Modeling of length distribution curves (during melt mixing)

Using a least-square fit, the amount of fiber (number fraction in percentage) having a fixed length in the composite prepared at a given mixing speed is found to follow the following relation:

$$D(\%) = A + Bl + Cl^2 \tag{1}$$

where D is the amount of fiber (number fraction in percentage) having a given length in percentage in the composite and l is the length of the fiber. A is a constant representing the total mechanical force distribution resulting from the rotor speed. The terms B and C represent the centrifugal and centripetal effects of the mixer on the upper, middle, and lower range sizes of the fillers.

Modeling of tensile properties

Several theories have been proposed to model the tensile properties of composite material in terms of different parameters.[34–37] In this article, we deal with theories of particulate and fibrous inclusions in a rigid matrix.

Modified rule of mixtures (MROM)

The modified rule of mixtures[38] can be given as follows:

$$T_c = T_m(1 - V_f) + T_f V_{fe} \tag{2}$$

where T_c is the ultimate strength of the composites; T_m, the matrix strength at the failure strain of the fiber; T_f, the ultimate strength of the fiber; V_f, the fiber-volume fraction; and V_{fe}, the effective fiber-volume fraction. The effective fiber-volume fraction is given in terms of the fiber-volume fraction and the ratio of real contribution as follows:

$$V_{fe} = V_f(1 - P) \tag{3}$$

where P is the degradation parameter for the effective fiber-volume fraction, lying between 0 and 1. P can be calculated from the microgeometry of the composite components and depends only on the fiber-volume fraction because the microgeometry is intimately related to the fiber-volume fraction under identical manufacturing conditions.

P can be calculated from the equation

$$P = \frac{\Delta T_c}{T_f V_f} \tag{4}$$

where ΔT_c is the difference between the experimentally measured strength and the strength predicted by the rule of mixtures.

Parallel and series models

The parallel and series models[39] are used to determine the modulus and tensile strength of short-fiber composites. The equations for tensile strength are

$$T_c = T_f V_f + T_m V_m \text{ (parallel model)} \tag{5}$$

$$T_c = \frac{T_m T_f}{T_m V_f + T_f V_m} \text{ (series model)} \tag{6}$$

where T_c, T_m, and T_f are the tensile strength of the composite, matrix, and fiber, respectively. If the modulus is the parameter under study, notations such as M_c, M_m, and M_f may be used instead of T_c, T_m, and T_f, where M_c, M_m, and M_f are the Young's moduli of the composite, matrix, and fiber, respectively.

Hirsch model

The Hirsch model[40] is a combination of parallel and series models. Using this model, the tensile strength and Young's modulus are determined by the equations

$$T_c = x(T_m V_m + T_f V_f) + (1 - x)\frac{T_f T_m}{(T_m V_f + T_f V_m)} \quad (7)$$

where x is a parameter which determines the stress transfer between the fiber and matrix.

In terms of the modulus, the equation is

$$M_c = x(M_m V_m + M_f V_f) + (1 - x)\frac{M_f M_m}{M_m V_f + M_f V_m} \quad (8)$$

Counto's model

The Counto model[41] for a two-phase system proposed by Counto is given by the equation

$$\frac{1}{E_c} = \frac{1 - V_f^{1/2}}{E_m} + \frac{1}{(1 - V_f^{1/2}); V_f^{1/2} E_m + E_f} \quad (9)$$

where E is the modulus; c, m, and f refer to the composite, matrix, and fiber, respectively; and V_f is the volume fraction of the fiber. This is applicable mainly to concrete systems. The schematic representations of the above four models are given in Figure 2.

Bowyer–Bader's model

According to Bowyer–Bader's[42] model, the tensile strength is given by

$$T_c = T_f K_1 K_2 V_f + T_m V_m \quad (10)$$

where K_1 is the fiber-orientation factor. Depending on the fiber orientation, K_1 also changes. K_2 is the fiber-length factor. For fibers with

$$l > lc, K_2 = l - lc/2l \quad (11)$$

For fibers with

$$l < lc, K_2 = l/2\ lc \quad (12)$$

where l is length of the fiber, and lc, its optimum length. According to the above model, the Young's modulus also can be calculated using the equation

$$M_c = M_f K_1 K_2 V_f + M_m V_m \quad (13)$$

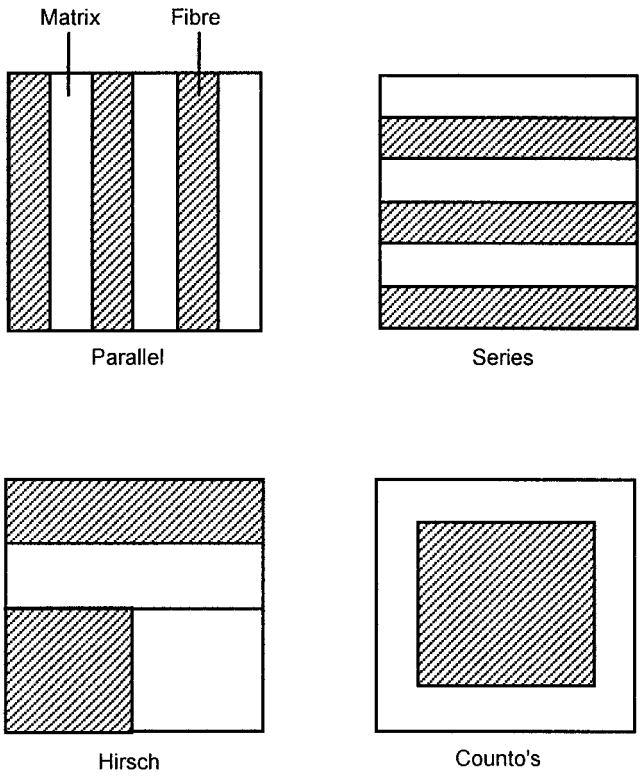

Figure 2 Schematic representation of parallel, series, Hirsch, and Counto's models.

Modeling of fiber orientation

The dependence of the angle of fiber orientation on the modulus or tensile strength of fiber composites can be studied using the equation[43]

$$\frac{1}{E_\theta} = \frac{\mathrm{Cos}^2\,\theta}{E_L} + \frac{\mathrm{Sin}^2\,\theta}{E_T} \quad (14)$$

where E_θ is the modulus of the composite wherein fibers deviate from the direction of test by the angle θ; E_L, the longitudinal composite modulus ($\theta = 0$); and E_T, the transverse composite modulus ($\theta = 90°$).

RESULTS AND DISCUSSION

Theoretical modeling of fiber-length distribution curves

Figure 3 depicts the fiber-length distribution curves showing the percentage amount (number fraction in percentage) of fiber having different lengths in the composite prepared at different mixing speeds. From the figure, it is very clear that the amount (number fraction in percentage) of fiber having small lengths increases with increase in the rotor speed (rpm). For example, the percentage of fiber with length of 2 mm or less at 50 rpm is 28.58; at 40 rpm, the value is 26.08; and at 30 rpm, it is 16.13. On the contrary, the per-

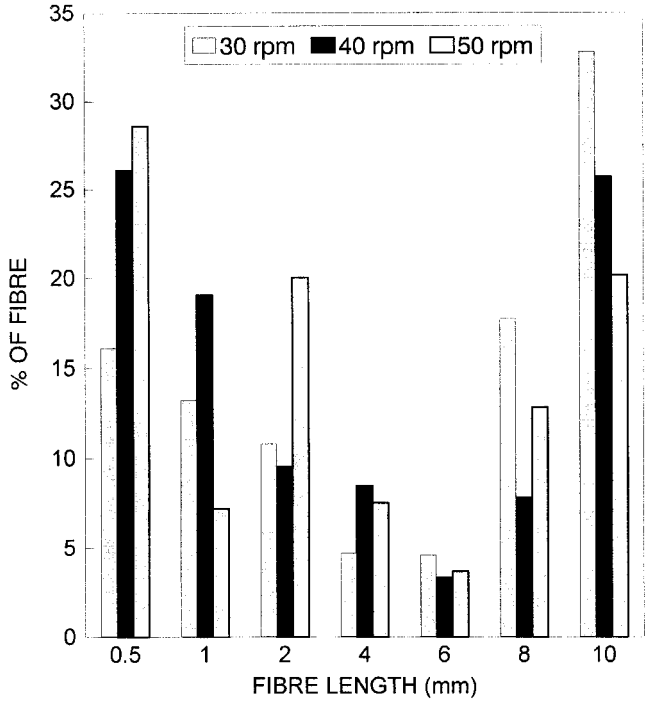

Figure 3 Fiber-length distribution curves showing the percentage amount of fiber having different lengths in the composite prepared at different mixing speeds.

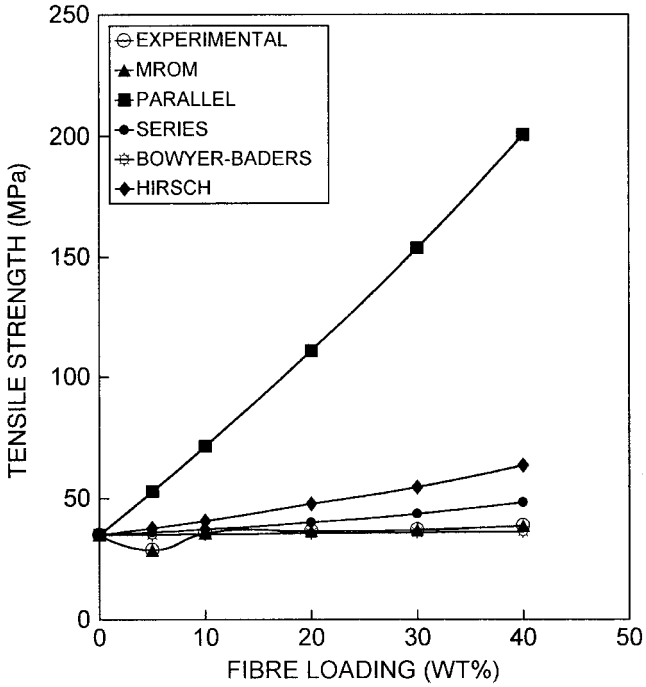

Figure 4 Experimental and theoretical curves for the variation of tensile strength against fiber loading for melt-mixed random sisal–PP composites (fiber length 6 mm).

centage of a 10-mm fiber is maximum at 30 rpm (i.e., at a low rotor speed).

The experimental data on the fiber-length distribution is found to fit nicely into a second-order polynomial equation [eq. (1)]. The values of the constants in eq. (1) for different mixing speeds are given in Table II. It is clear that the effect of increasing the rotor speed results in an increase in the value of A. This increased mechanical stress due to increased rotor speed results in more and more distribution for smaller lengths and an opposite trend for bigger fiber lengths, that is, as the rotor speed increases, the amount of fibers having small lengths increases.

Theoretical modeling of tensile properties

Figure 4 gives a comparison of the variation in the experimental and theoretical tensile strength values of melt-mixed random composites with fiber loading (fiber length, 6 mm; temperature, 170°C; rpm, 50). It is interesting to note that, in all cases, the tensile strength increased with increase in the volume fraction of the fibers. On analyzing the figure, it is very clear that the experimental value exactly fits with the theoretical value in the case of the modified rule of mixtures. It can be assumed that the model (modified rule of mixtures) predicts the actual composite strength because the value of P in eq. (4) is defined to account for the microgeometry of real composites.[38] At a low fiber content, the fiber may act as a flaw in the matrix (plasticization effect), reducing the tensile strength of the composite.[31] Next to MROM, the Bowyer–Bader model, the series model and the Hirsch model showed good agreement with the experimental tensile-strength values. At low fiber loading, these models are in close agreement with the experimental tensile-strength value, but as the volume fraction of the fiber increases, the extent of deviation from the experimental value also increases. The agreement in tensile-strength values of the various theoretical models with that of the experimental values is in the order MROM > Bowyer–Bader > series > Hirsch > parallel. The deviations exhibited by the system are due to the difference in the mode of stress transfer in short-fiber composites. In the case of short-fiber composites, the stress transfer is a function of fiber orientation, stress concentration at fiber ends, optimum fiber length, etc. When the concentration of the fiber in the matrix is low, stress will be uniformly distributed in the composite and, consequently, satisfactory agreement between theoretical and experimental values is ob-

TABLE II
Values of the Constants A, B, and C in Eq. (1) for Different Mixing Speeds (Rotor Speeds)

No.	Speed (rpm)	A	B	C
1	30	20.47	−7.6	0.88
2	40	29	−9.7	0.95
3	50	32.70	−9.42	0.825

served. But as the concentration of fiber increases, fiber agglomeration predominates, which causes an uneven distribution of the applied load in the composite. Since this factor is not accounted for by the models, they deviate from the experimental value to different extents.

From the study, it is also clear that the value of "x" in the Hirsch model, which is a function determining the efficient stress transfer, has some role in predicting the correct experimental tensile strength. The best correlation between theoretical and experimental values was obtained when the value of x is 0.1. Further reduction in the x value is found to decrease the tensile-strength values only to the fourth decimal place, which is not prominent as far as tensile strength is concerned. In the Bowyer–Baders model, tensile strength is calculated using eq. (15), which depends upon two factors: K_1, the fiber-orientation factor, and K_2, the fiber-length factor. The agreement between theoretical and experimental values was found only when the values of K_1 and K_2 were 0.2 and 0.33, respectively. In this case, the value of K_1, for good agreement between theoretical and experimental values, was found to be 0.2, because it has already been reported that the value of K_1 for fibers arranged in a random fashion is 0.2.[45] K_2 is calculated using eq. (16) since l = 6 mm and l_c = 2 mm.[31] Usually, parallel and series models are used to describe the strength of continuous fiber-reinforced polymeric composites. In the case of the parallel model, it is assumed that iso-strain conditions exist for both matrix and fiber, whereas in the case of a series model, stress was assumed to be uniform in both the matrix and fiber.[41] The assumption of either uniform stress or uniform strain is clearly an oversimplification in this case. The stress-transfer mechanism of continuous fiber-reinforced composites is different from that of short-fiber composites.

The Young's modulus values of melt–random-mixed (170°C) composite samples are compared with the theoretical prediction in Figure 5. It is very clear from the figure that the tensile modulus of randomly oriented composites show a reasonable agreement with all the models at low fiber concentrations. This may be due to uniform distribution of an applied load as a result of well-dispersed fibers in the matrix at low fiber concentrations. But as the fiber concentration increases, theoretical models deviate from the experimental value to different extents. This may be due to fiber agglomeration and fiber–fiber interactions at higher fiber loadings. In all cases of fiber concentrations, it is interesting to see that the series, the Bowyer–Bader, and the Hirsch models are in good agreement with the experimental values, although the Hirsch model shows a slight positive deviation, while the series and Bowyer–Bader models exhibit a negative deviation. In the case of the Hirsch model, the value of x = 0.1 is selected because it gives good agreement with the experimental values for randomly oriented composites.

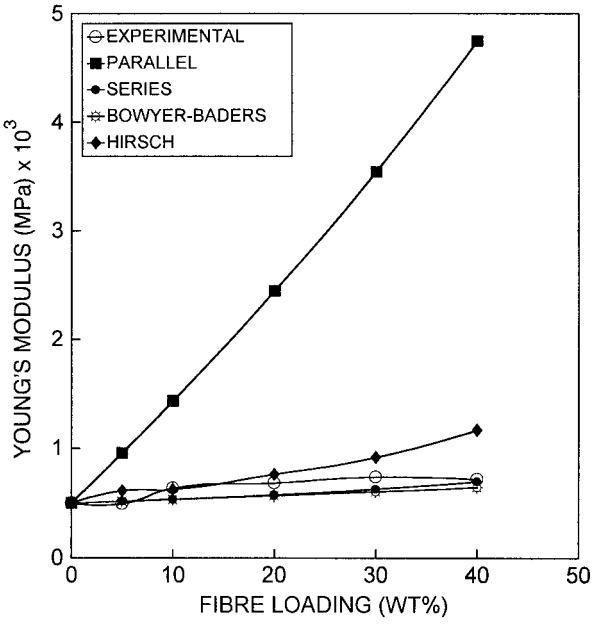

Figure 5 Experimental and theoretical curves for the variation of the Young's modulus against fiber loading for melt-mixed random sisal–PP composites (fiber length 6 mm).

Theoretical modeling of tensile properties of chemically treated fiber composites

When sisal fibers are subjected to chemical treatment using PMPPIC, the hydrophilicity of the fiber is reduced. This results in a better compatibility between the fiber and the PP matrix, thereby increasing the tensile properties of the composite. A possible hypothetical chemical structure of the bonding of PMPPIC at the interfacial area of the sisal fiber and PP is given in Figure 6.

When the fiber surface is modified by a polymeric interphase, interdiffusion between PP and cellulose fibers might be expected, leading to increased tensile strength of the composite. The longer the chain of the modifier, the better are the tensile properties of the composite. The longer, flexible chain of PMPPIC is able to diffuse deeper into the matrix, and PP becomes involved more fully in the interchain entanglements.[44] This contributes to the enhanced mechanical performance of the system.

Figure 7 represents the experimental and theoretical curves of the tensile strength of the composite (PMPPIC-treated) as a function of fiber loading. It is interesting to note that the experimental values exactly fit with the values suggested by the modified rule of mixtures at all fiber loadings. A good correlation between the theoretically and experimentally observed tensile strength was seen in the case of the series,

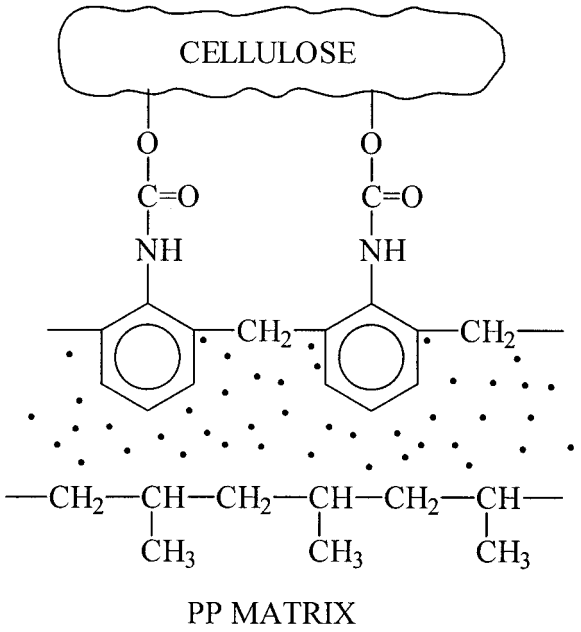

Figure 6 Possible hypothetical chemical structure of bonding of PMPPIC at the interfacial area of sisal fiber and PP.

Hirsch, and Bowyer–Bader models, although these models show a slight deviation from the experimental values. Although the parallel model shows positive deviation, the deviation is less compared to the untreated fiber composites, which can be understood from Figure 4. Figure 8 shows the experimental and theoretical curves of the Young's modulus of the PMPPIC-treated composite as a function of fiber loading. Similar to the tensile strength, the tensile modulus also increases in the case of the PMPPIC-treated sisal fiber composite compared to untreated composites. Since the tensile modulus increases to high values, it is in close agreement with the parallel model at certain concentrations rather than to any other models.

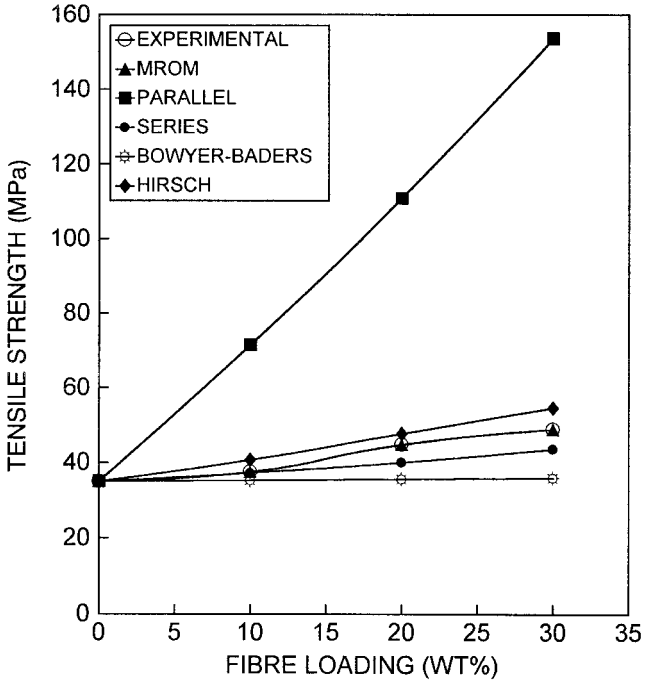

Figure 7 Experimental and theoretical curves of tensile strength against fiber loading (PMPPIC-treated) for melt-mixed random sisal–PP composite (fiber length 6 mm).

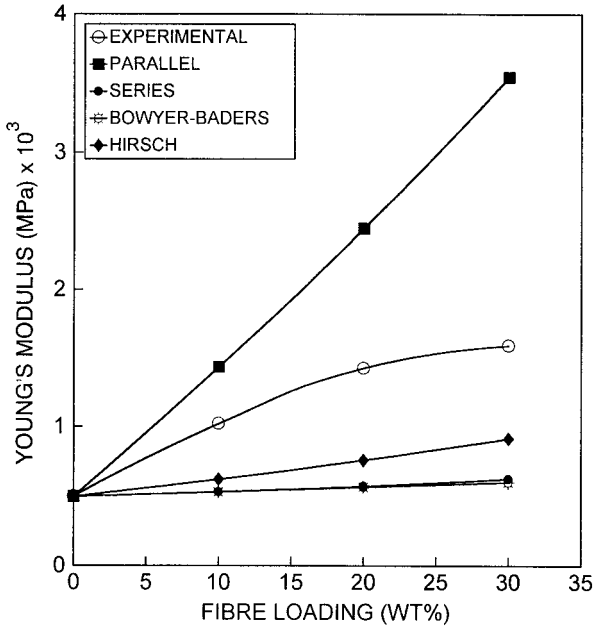

Figure 8 Experimental and theoretical curves of the Young's modulus as a function of fiber loading (PMPPIC-treated) for melt-mixed random sisal–PP composite (fiber length 6 mm).

Theoretical modeling of fiber-length effect on tensile properties

The relationship between the length and properties of a short fiber-reinforced polymeric matrix deserves much importance experimentally and theoretically. Figure 9 represents the tensile strength–fiber length plots of melt-mixed random fiber composites (both experimental and theoretical). In the present study, MROM and the modified Bowyer–Baders models were used for the calculation of the tensile strength. The optimum fiber length was found to be 2 mm from an earlier study.[31] Hence, other lengths such as 1 mm are taken as subcritical, while 6, 10, and 15 mm, as supercritical lengths. In all the cases, the concentration of the fiber in the composite was 20%. The MROM exactly fits with the experimental values at all fiber lengths (as explained earlier). The Bowyer–Bader model is in good agreement with the experimental values.

Tensile properties were calculated using eqs. (15) and (18) and they depend upon the value of K_2 since it is the fiber-length factor. The value of K_2 in eqs. (15)

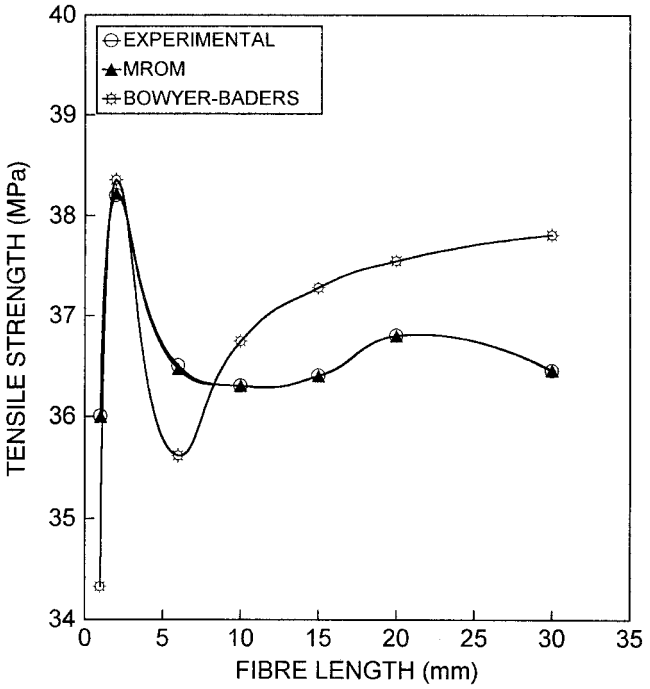

Figure 9 Experimental and theoretical curves of tensile strength against fiber length in the case of melt-mixed random composites (fiber loading 20%).

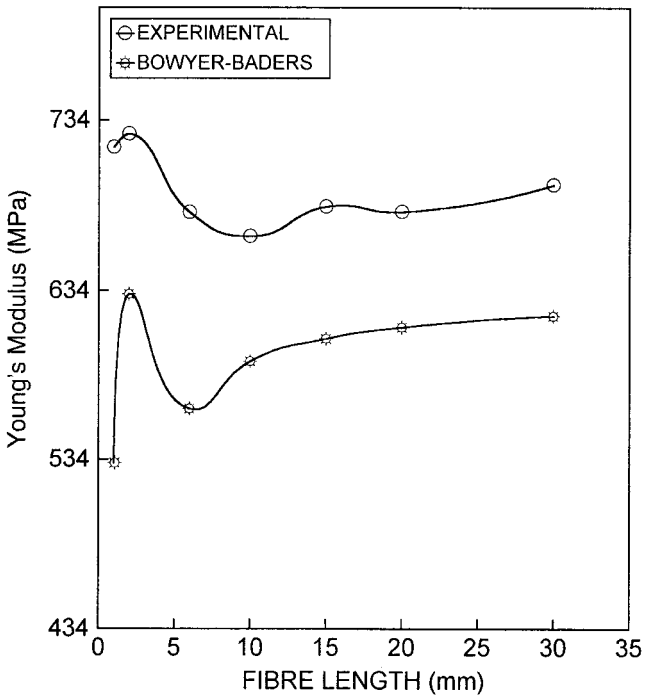

Figure 10 Experimental and theoretical curves of the Young's modulus against fiber length in the case of melt-mixed random composites (fiber loading 20%).

and (18) is different for different fiber lengths. For 1-mm fibers, the value of K_2 was calculated using eq. (17), and for 6-, 10-, 15-, 20-, and 30-mm fibers, K_2 was calculated using eq. (16). As fiber length increases, the possibility of entanglement also increases. Moreover, it is observed that as the fiber length is minimum the fiber can pack effectively and can give better tensile properties. Thus, at a low fiber length (2 mm), the tensile strength is high and it is close to that of the Bowyer–Baders model. As the fiber length increases, the theoretical values deviate more and more from the experimental values.

Figure 10 represents the modulus–fiber length plots of melt-mixed random fiber composites. The Bowyer–Bader model is used to calculate the tensile modulus. It is very clear from Figures 9 and 10 that at a 2-mm fiber length there is fairly good agreement between the theoretical and experimental values in the case of tensile strength and tensile modulus values. This clearly indicates that at an optimum fiber length the composite shows maximum properties.

Theoretical modeling of angular dependence of composite tensile properties

Figure 11 represents the experimental and theoretical plots of the tensile strength of solution-mixed composites as a function of the angle of measurement with respect to the fiber orientation. Equation (19) applies to situations when property measurement is done with different angles to the longitudinal orientation ($\theta = 0°$). At 10% fiber concentration, it can be seen that there is good agreement between the experimental

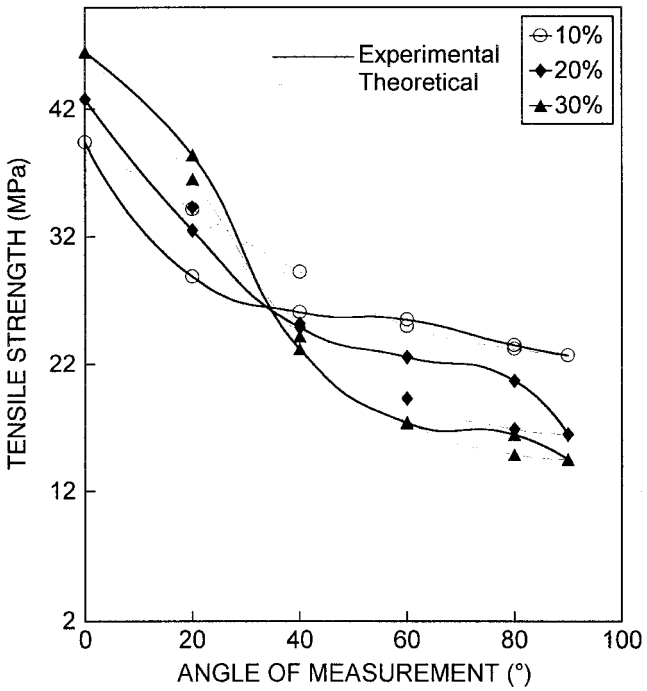

Figure 11 Experimental and theoretical plots of tensile strength of solution mixed sisal–PP composites of a function of the angle of measurement with respect to fiber orientation (fiber length 6 mm) at different fiber loadings.

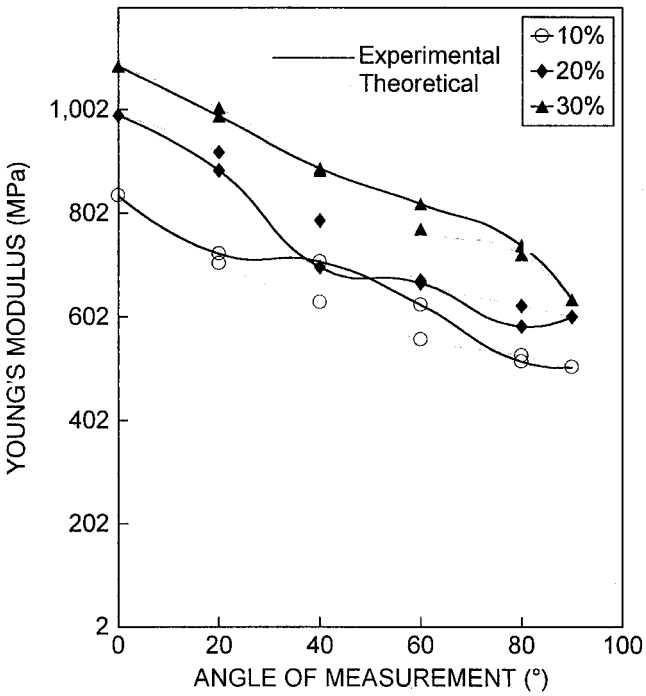

Figure 12 Experimental and theoretical plots of the Young's modulus of solution mixed sisal–PP composites as a function of the angle of measurement with respect to fiber orientation (fiber length 6 mm) at different fiber loadings.

and theoretical plots. The deviation is maximum at lower degrees. At 20% fiber loading, the best fit is observed at 40°. When the fiber concentration is 30%, good agreement between the experimental and theoretical values is obtained at most of the angles, especially at 40 and 60°. It can be generally seen that eq. (19) successfully presents the variation in the experimental tensile strength with the fiber orientation angle. At longitudinal ($\theta = 0$) and transverse ($\theta = 90°$) orientation, experimental and theoretical values merge into a single value.

Similar plots for the Young's modulus of the composites are presented in Figure 12. At low fiber loading (10%), the best agreement was observed at 20 and 80°. In the case of 20% fiber loading, the best agreement between experimental and theoretical values are observed at 60°. It is surprising to see the good agreement between the theoretical and experimental values at all the angles for the composite containing 30% sisal fiber. These plots reveal the considerable sensitivity of the modulus to the fiber orientation experimentally and theoretically. It also clarifies the significance of good orientation for achieving high moduli. In general, it can be concluded that the equation is able to reflect the anisotropy in the tensile properties of fiber-reinforced PP composites.

Deviation from the models

As we have already seen, many models deviate from the experimental results. This is because of various reasons such as the presence of voids, fiber–fiber interaction at higher loadings, and poor fiber–matrix interaction. The chance of the formation of microvoids between the fiber and matrix during the preparation of the composites greatly influences the tensile properties. At higher fiber loadings, there is a chance of fiber agglomeration, which also influences the tensile properties of the composites. Sisal fiber is hydrophilic and the PP matrix is hydrophobic. So, the resulting sisal/PP composite is incompatible, giving rise to poor fiber–matrix adhesion. This may contribute to a poor stress transfer between the matrix and the fiber, leading to unsatisfactory tensile properties. These factors are not accounted for in any of the models used in the study. Moreover, most of the models assume a cylindrical shape for the fibers while sisal fiber is not perfectly cylindrical due to surface irregularities, which is evident from Figure 13(a). The chance of formation of

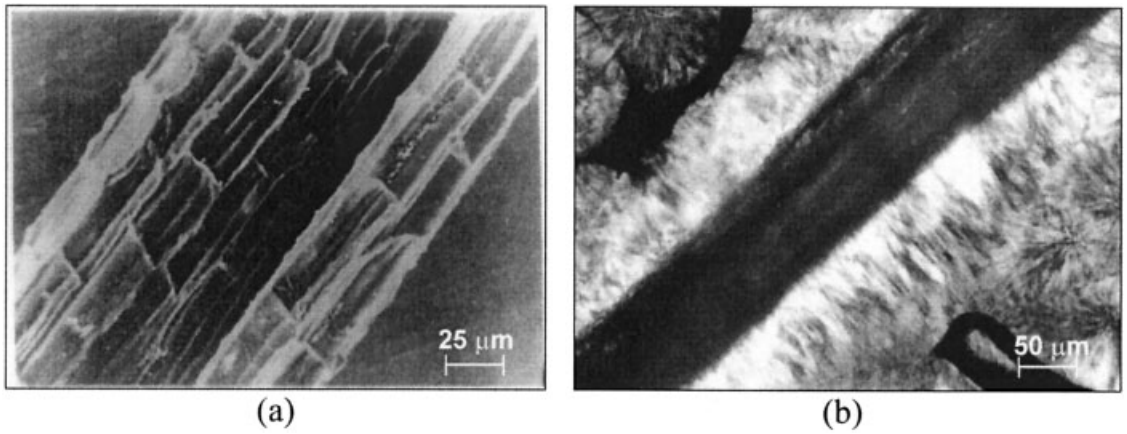

Figure 13 (a) Scanning electron micrograph of the surface of the sisal fiber. (b) Optical photomicrograph showing transcrystallinity at the interphase between fiber and PP in the composite.

transcrystallinity [Fig. 13(b)] at the fiber matrix interface also affects the tensile properties of the composites, which is not accounted for any of the above models. Since the models used in the study do not account for the presence of voids, fiber–fiber interactions, nonuniform shape of the sisal fiber, poor fiber–matrix interaction, and formation of transcrystallinity at the interphase between the fiber and the matrix, the models show some deviations from the experimental behavior.

CONCLUSIONS

A comparison was made between the experimental results and the theoretical calculations from various models on the fiber-length distribution, tensile properties with fiber loading, and fiber orientation (angle of measurement) in the case of short sisal fiber-reinforced PP composites. Fiber-length distribution curves were modeled using a polynomial equation. Tensile properties of both solution-mixed (random) and melt-mixed (random only) composites were studied. The polynomial equation was found to be successful to model the fiber-length distribution. The various theoretical models used were MROM, parallel, series, Hirsch, and Bowyer–Bader. In the case of the series model, stress was assumed to be uniform in both the matrix and the fiber.[34] This condition can be satisfied fully in the case of longitudinally oriented fiber composites. That is why there is close agreement with the experimental and theoretical values in the case of the series model. The parallel model deviates the maximum from the experimental value in most of the cases. The experimental and theoretical relationship between the length and the tensile properties of short sisal fiber-reinforced PP was studied. All the equations predicted superior tensile performance at the optimum length of the sisal fiber. The anisotropy in tensile strength and modulus with the angle of fiber orientation was studied and found to be in good agreement with the theoretical data. Finally, it is important to mention that the deviation observed in the case of experimental values from the theoretical values is due to the presence of voids, fiber–fiber interactions, nonuniform shape of the sisal fiber, poor fiber–matrix adhesion, and formation of transcrystallinity at the interphase between the fiber and the matrix.

References

1. Joly, C.; Gauthier, R.; Escouben, M. J Appl Polym Sci 1996, 61, 57.
2. Woodhams, R. T.; Thomas, G.; Rodgers, D. K. Polym Eng Sci. 1984, 24, 1166.
3. Sotton, M.; Ferrari, M. Ind Text 1989, 1197, 58.
4. Karmaker, A. C.; Hoffmann, A.; Hinrichsen, G. J Appl Polym Sci 1994, 54, 1803.
5. Cruz-Ramos, C. A. In Mechanical Properties of Reinforced Thermoplastics, Clegg, D. W., Collyer, A. A., Eds.; Elsevier: New York, 1986; pp 65–81.
6. Setua, D. K. Polym Commun 1984, 25, 345.
7. Murthy, V. M.; De, S. K. J Appl Polym Sci 1984, 29, 1355.
8. Moghe, S. R. Rubb Chem Technol 1976, 49, 1160.
9. Folkes, M. J. Short Fiber Reinforced Thermoplastic Composites; Wiley: New York, 1982.
10. Nielsen, L. E. Mechanical Properties of Polymers and Composites; Van Nostrand Reinhold; New York, 1973; Vol. 2.
11. Bledzki, A. K.; Reihmane, S.; Gassan, J. J Appl Polym Sci 1996, 59, 1329.
12. Gassan, J.; Bledzki, A. K. Compos A 1997, 28, 1001.
13. Pavithran, C.; Mukherjee, P. S.; Brahmakumar, M.; Damodaran, A. D. J Mater Sci Lett 1987, 6, 882.
14. White, N. M.; Ansell, M. P. Mater Sci 1983, 18, 1549.
15. Varma, D. S.; Varma, V.; Varma, I. K. Text Res J 1984, 54, 827.
16. Raj, R. G.; Kokta, B. V.; Maldas, D.; Daneault, C. J Appl Polym Sci 1989, 37, 1089.
17. Raj, R. G.; Kokta, B. V.; Maldas, D.; Daneault, C. Makromol Chem Macromol Symp 1989, 28, 187.
18. Maldas, D.; Kokta, B. V. J Comp Mater 1991, 25, 375.
19. Maldas, D.; Kokta, B. V. J Appl Polym Sci 1990, 40, 917.
20. Maldas, D.; Kokta, B. V.; Daneault, C. J Appl Polym Sci 1989, 37, 751.
21. Raj, R. G.; Kokta, B. V.; Daneault, C. Int J Polym Mater 1989, 12, 235.
22. Maldas, D.; Kokta, B. V. Comp Sci Technol 1989, 36, 167.
23. Felix, J. M.; Gatenholm, P. J Appl Polym Sci 1991, 42, 609.
24. Paramasivan, T.; Abdulkalam, A. P. J Fiber Sci Technol 1974, 7, 85.
25. Joseph, K.; Thomas, S.; Pavithran, C.; Brahmakumar, M. J Appl Polym Sci 1993, 47, 1731.
26. Joseph, K.; Pavithran, C.; Thomas, S. Eur Polym J Nat Rubb Res 1991, 4, 55.
27. Varghese, S.; Kuriakose, B.; Thomas, S.; Koshy, A. T. Ind J Natl Rubb Res 1991, 4, 55.
28. Varghese, S.; Kuriakose, B.; Thomas, S.; Koshy, A. T. Ind J Natl Rubb Res 1992, 4, 55.
29. Manikandan Nair, K. C.; Diwan, S. M.; Thomas, S. J Appl Polym Sci 1996, 60, 1483.
30. George, J.; Bhagawan, S. S.; Prabhakaran, N.; Thomas, S. J Appl Polym Sci 1995, 57, 843.
31. Joseph, P. V.; Joseph, K.; Thomas, S. Compos Sci Technol 1999, 59, 1625.
32. Joseph, P. V.; Joseph, K.; Thomas, S. Compos Interf, In Press.
33. Joseph, K.; Thomas, S.; Pavithran, C.; Brahmakumar, M. J Appl Polym Sci 1993, 47, 1731.
34. Robinson, I. M.; Robinson, J. M. J Mater Sci 1995, 29, 4663.
35. Sarasua, J. R.; Remiro, P. M.; Pouyet, J. J Mater Sci 1995, 30, 3501.
36. Kelley, A.; Tyson, W. R. J Mech Phys Solids 1965, 13, 329.
37. Chawla, K. K. Composites in Materials Science and Engineering; Springer: New York, 1987; p 177.
38. Lee, C.; Hwang, W. J Mater Sci 1998, 17, 1601.
39. Broutman, L. J.; Krock, R. M. Modern Composite Materials; Addison-Wesley: Reading, MA, 1967.
40. Hirsch, T. J. J Am Com Inst 1962, 59, 427.
41. Counto, U. J. Mag Conc Res 1964, 16, 129.
42. Bowyer, W. H.; Bader, M. G. J. Mater Sci 1972, 7, 1315.
43. Coran, A. Y.; Baustany, K.; Hamed, P. J Appl Polym Sci 1971, 15, 2471.
44. George, J.; Bhagawan, S. S.; Thomas, S. Compos Interf 1998, 5, 201.